ACS Photonics

Letter

Cite This: ACS Photonics 2019, 6, 844−850

pubs.acs.org/journal/apchd5

Ultrafast All-Optical Light Control with Tamm Plasmons in Photonic Nanostructures

Boris I. Afinogenov,*[,†] Vladimir O. Bessonov,[†,‡] Irina V. Soboleva,[†,‡] and Andrey A. Fedyanin[†]

[†]Faculty of Physics, Lomonosov Moscow State University, Moscow 119991, Russia

[‡]Frumkin Institute of Physical Chemistry and Electrochemistry, Russian Academy of Sciences, Moscow 119071, Russia

Supporting Information

ABSTRACT: Ultrafast all-optical modulators are crucial parts of prospective photonic devices. A number of plasmonic and dielectric nanostructures were nominated as candidates for integrated all-optical circuits. The key principle in the design of such devices is to engineer artificial optical resonances to increase the magnitude of modulation or to change the characteristic switching time. The major drawback is that the manufacturing becomes rather sophisticated. Here, we propose a method to tailor the ultrafast response of photonic crystal−metal nanostructures by employing a spectral shift of the Tamm-plasmon resonance. We show that for the absorbed pump fluence of 6 pJ reflectance of the sample at the near-infrared probe wavelength in the vicinity of the Tamm-plasmon resonance changes 25× stronger as compared with a bare metal film. Additionally, we show that by choosing a proper wavelength around the resonance a background-free reflectance modulation can be achieved. The characteristic pulse-limited switching time, in this case, is 150 fs.

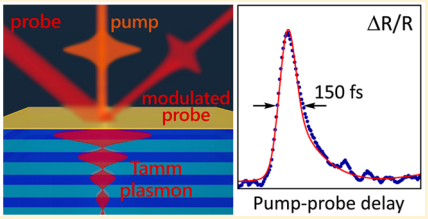

KEYWORDS: *plasmonics, all-optical switching, carrier dynamics, femtosecond optics, photonic crystals, Tamm plasmons*

Optical data processing is now considered as one of the most prospective methods to succeed modern electronics. A significantly smaller level of heating and energy consumption, along with the extremely high operation speed, fosters development of the efficient all-optical modulators and switches. Over the past decades, several approaches were proposed to achieve pronounced ultrafast modulation of optical signals. One of the most developed is a plasmonic approach which utilizes metallic nanostructures to couple, guide, and manipulate light. It was shown that metallic nanoparticles,[1−4] plasmonic crystals,[5,6] and hybrid plasmonic nanostructures[7−9] yield a relative change in reflectance or transmittance of up to 100%. Characteristic times of switching were in the order of several picoseconds for large modulations and several hundred femtoseconds for a few-percent modulation. Another approach, gaining much attention now relates to all-dielectric nanonstructures. It was first proposed for photonic crystals (PCs)[10−12] and then expanded to dielectric nanoparticles[13,14] and semiconductor metasurfaces.[15−17]

All the methods rely on engineering artificial resonances which spectral positions are sensitive to the material properties or the geometry of nanostructure. The idea is that changing the complex permittivity of materials composing the sample leads to the spectral shift of the resonance and increase of the relative change in the sample reflectance or transmittance. The bandwidth of the nanophotonic switch is determined by the physical processes, responsible for the permittivity change. The rule of thumb is that fast nonlinear processes such as two-photon absorption and Kerr nonlinearity yield bandwidths of up to 10 THz but induce small modulations of optical response,[15] while slow processes involving free-carrier generation lead to the significant change of the optical response,[18] but the bandwidth usually does not exceed 50 GHz. When plasmonic systems are considered, the most substantial modulations of reflectance and transmittance are observed if the light frequency is close to the plasma frequency of metal.[19] In contrast, when the more preferable for applications infrared radiation is used, the change of reflectance or transmittance usually does not exceed 1%.[20,21]

Hybrid photonic crystal−metal structures give an ability to overcome this issue. They provide an additional degree of freedom, related to the geometry of photonic crystal. It was shown that PC−metal nanostructures support excitation of Tamm plasmons (TPs) in the infrared part of the spectrum.[22] TPs can be excited at normal incidence of light and their resonant frequency experiences blueshift and polarization splitting upon increasing the angle of incidence.[23] The spectral position of the TP resonance is also affected by thicknesses of PC layers and metal film.[24,25] Excitation of the TP leads to the electromagnetic field localization at the interface of a PC and metal. Thus, TPs can form hybrid states with surface and localized plasmons,[26] cavity modes,[27] and excitons.[28] Field localization and sensitivity to the small variations in the sample geometry stipulated exploitation of TPs in novel lasers,[29,30] nonlinear devices,[31−33] sensors,[34−36] and emitters.[37−40]

In this Letter, we demonstrate how Tamm plasmons can tailor the ultrafast optical response of photonic−plasmonic nanostructures in the near-infrared range. We study exper-

Received: December 28, 2018
Published: March 5, 2019

DOI: 10.1021/acsphotonics.8b01792
ACS Photonics 2019, 6, 844−850

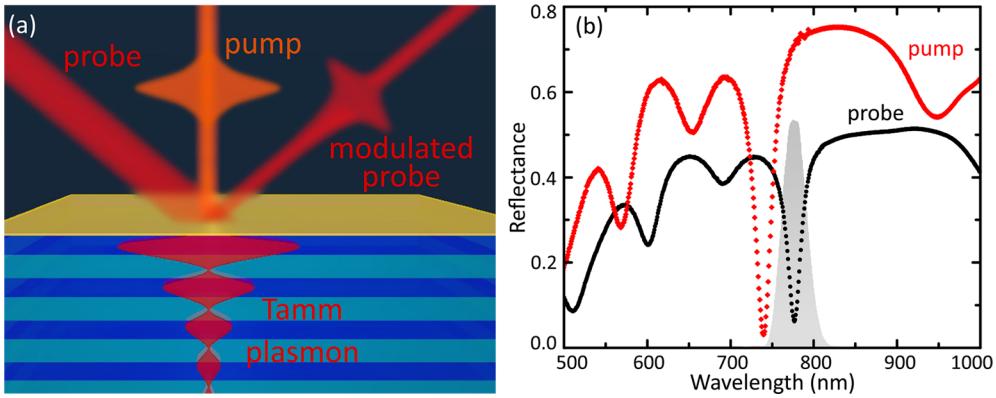

Figure 1. (a) Sketch of the experiment. (b) Reflectance spectra of the sample at angles of incidence of 20° (black dots) and 45° (red dots) corresponding to the probe and pump incident angles, respectively. The shaded area represents the spectrum of pump and probe laser pulses.

imentally the transient reflectance and transmittance of a one-dimensional photonic crystal covered with a 30 nm thick gold film. Using time-resolved spectroscopy, we demonstrate that the temporal dynamics of reflectance and transmittance of the PC−metal sample depends significantly on the probe wavelength around TP resonance. The proper selection of the probe wavelength leads to a background-free pulse-limited modulation of reflectance and transmittance. Modifying gold complex permittivity by a low-power infrared pump, we achieve switching with a characteristic time of 150 fs.

RESULTS AND DISCUSSION

The studied sample was a $(ZrO_2/SiO_2)_6$ photonic crystal (quarter-wavelength distributed Bragg reflector) covered with a 30 nm thick gold film. The outline of the experiment is shown in Figure 1a. Probe radiation (red) is in resonance with the Tamm-plasmon mode, so the reflected intensity is low. After a femtosecond pump pulse (orange) transfers energy to electrons in gold, its complex permittivity changes. TP resonance spectrally shifts and reflectance of the probe changes. Temporal dynamics of the probe reflectance depends on several parameters which are discussed further.

Measurements were performed in a pump−probe scheme with cross-polarized pump and probe beams. A femtosecond pulse from Ti:sapphire laser was split into two channels with the intensity ratio of pump and probe being 30:1. Then two beams were independently focused on the sample with parabolic mirrors. Reflected probe beam was passed to a monochromator which allowed to perform wavelength-resolved measurements in the range of the femtosecond pulse spectrum (full width at half-maximum = 25 nm). The explicit scheme of the experimental setup is given in the Supporting Information, section 1. For the measurements, we have chosen the strategy of the TP-resonant probe and off-TP-resonant pump. To realize this, probe and pump radiation were incident on the sample at 20° and 45°, respectively. Figure 1b shows reflectance spectra of the sample at pump and probe incident angles along with the spectrum of the incident pulse.

Reflectance spectra of both pump and probe exhibit TP resonances, which are spectrally separated by 40 nm due to the TP angular selectivity. The spectrum of the Ti:sapphire laser pulse overlaps with the TP resonance at the probe angle of incidence and appears at the photonic bandgap at the pump angle of incidence. The employed scheme allowed for neglecting the change in the pump absorption during the shift of the TP resonance. The absorbed pump fluence was 2 $\mu J/cm^2$ equivalent to 6 pJ per pulse. All measurements were performed when the sample had thermally equilibrated after the initial long-term heating as discussed in the Supporting Information, section 2.

Relative change in reflectance $\Delta R/R$ and transmittance $\Delta T/T$ of the PC−metal sample can be directly related to the change in metal complex permittivity $\Delta\hat{\varepsilon}_{Me} = \Delta\varepsilon' + i\Delta\varepsilon''$ as

$$\frac{\Delta R}{R}(\lambda, \tau) = \frac{\partial \ln R(\lambda)}{\partial \varepsilon'}\Delta\varepsilon'(\tau) + \frac{\partial \ln R(\lambda)}{\partial \varepsilon''}\Delta\varepsilon''(\tau),$$
$$\frac{\Delta T}{T}(\lambda, \tau) = \frac{\partial \ln T(\lambda)}{\partial \varepsilon'}\Delta\varepsilon'(\tau) + \frac{\partial \ln T(\lambda)}{\partial \varepsilon''}\Delta\varepsilon''(\tau) \quad (1)$$

where λ is a probe wavelength and τ is a time delay between pump and probe pulses. We assume here that $\Delta\varepsilon$ does not depend on the wavelength, since we are working in a narrow spectral range far from gold intrinsic resonances. To improve readability we also denote $\alpha' = \partial \ln R/\partial\varepsilon'$, $\alpha'' = \partial \ln R/\partial\varepsilon''$, $\beta' = \partial \ln T/\partial\varepsilon'$, and $\beta'' = \partial \ln T/\partial\varepsilon''$.

As it was shown in refs 19 and 41, evolution of gold permittivity can be described as three consecutive processes with different time scales. The first stage after the pump pulse absorption is the formation of a nonequilibrium electron distribution. It is followed by thermalization and a cooldown due to electron−electron and electron−phonon interactions. Both real and imaginary parts of the transient permittivity are defined by the amount of the excess energy in the electron subsystem. Thus, their dynamics have characteristic times of several picoseconds as it is determined by the electron−phonon relaxation time. However, $\Delta\varepsilon''(\tau)$ has an additional contribution from the interband absorption in the non-equilibrium phase. For a gold film, this contribution takes the form of a pulse-limited spike if pump and probe wavelengths are in the near-infrared region. Procedure and the results of the numerical modeling of $\Delta\hat{\varepsilon}(\tau)$ for our case can be found in the Supporting Information, section 3.

The coefficients in eq 1 for a bare gold film are almost independent of the probe wavelength provided that the latter is far below the interband transition threshold. In this case, the transient reflectance of the gold is determined by both the $\Delta\varepsilon'$ and $\Delta\varepsilon''$ as the corresponding coefficients have comparable magnitude and the same sign. The transient transmittance takes the shape of the $\Delta\varepsilon'(\tau)$ which coefficient is three times larger than the one of $\Delta\varepsilon''$. As a result, ultrafast features of $\Delta\varepsilon''$ are not visible in transient reflectance and transmittance of a

DOI: 10.1021/acsphotonics.8b01792
ACS Photonics 2019, 6, 844−850

bare gold film, since they are obscured by smoother and larger changes of ε'.

The picture changes completely when an artificial resonance is introduced into the system. Figure 2 shows an experimental

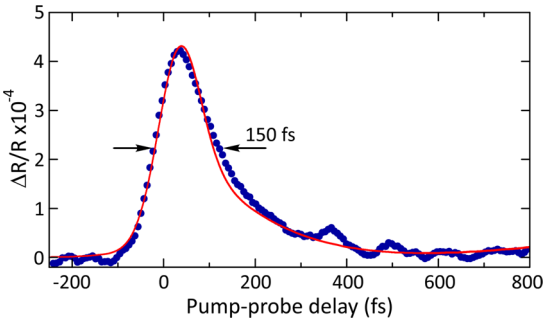

Figure 2. Transient reflectance of the PC−metal sample at the probe wavelength of 774.5 nm. Solid curve shows the result of the numerical calculation.

demonstration of a pulse-limited background-free modulation of reflectance of the PC−metal sample at the probe wavelength λ_0 = 774.5 nm. The sample reflectance shows a fast positive modulation and completely relaxes to the unperturbed value after 500 fs. The full width at half-maximum of the modulation spike is 150 fs and is determined by the pump−probe cross-correlation.

To explain the observed phenomenon, we recall that the studied PC−metal sample supports the excitation of Tamm plasmon at the wavelength of 776 nm. TP manifests itself as Lorentz-shaped resonances in spectra of reflectance and transmittance. As it was mentioned earlier, the spectral position and the shape of the TP resonance are sensitive to complex permittivities of materials composing the sample. It essentially means that spectra of coefficients in eq 1 have the complex line shape at wavelengths in the vicinity of the TP resonance. Indeed, assuming spectral shift of the TP resonance, the reflectance of the sample grows at one side of the resonance and falls at the other side. In other words, α' and α'' become sign-changing. The derivation and spectra of α and β coefficients for the studied sample are given in the Supporting Information, section IV.

At the wavelength λ_0, coefficients α' and α'' have different signs and such magnitudes that $|\alpha''/\alpha'| = \Delta\varepsilon'/\Delta\varepsilon''_{\text{intra}}$, where $\varepsilon''_{\text{intra}}$ is an intraband contribution to the gold permittivity. Consequently, the $\Delta R/R$ is determined mainly by the interband contribution to $\Delta\varepsilon''$. The interband term is a result of electron transitions from the gold *d*-band to the *sp*-band. In our experiment the probe photon energy $\hbar\omega_{\text{pr}}$ is less than the interband transition threshold $\hbar\Omega_{\text{ib}}$, so interband transitions can not take place in the unoccupied states above Fermi energy. However, the total energy of pump and probe photons being $\hbar\omega_{\text{pp}} + \hbar\omega_{\text{pr}}$ = 3.2 eV exceeds the $\hbar\Omega_{\text{ib}}$ = 2.4 eV. Thus, the interband transitions occur from the top of the *d*-band to the states far from Fermi energy which are depleted by the pump pulse. As these states are short-living, interband transitions occur only when the pump and probe photons arrive almost simultaneously. Thus, the $\Delta\varepsilon''_{\text{ib}}(\tau)$ closely follows the pump−probe cross-correlation.

The modulation of the gold complex permittivity leads to the modification of the TP resonance as schematically shown in the inset of Figure 3a. Dots in Figure 3a show the measured values of the sample $\Delta R/R(\lambda)$ at the time delay of +200 fs when the ultrafast modulation has almost finished. The gray line in the same figure shows the TP-resonance line shape. The redshift and spectral broadening of the TP resonance give rise to the asymmetrical derivative-like spectrum of the change in reflectance.

The largest modulation is obtained at the wavelengths of 771 nm (pink dot) and 779 nm (red dot) corresponding to the slopes of the resonance. In contrast, at the wavelengths close to the TP resonance minimum (blue, cyan, and orange dots), $\Delta R/R$(+200 fs) is almost zero as its dynamics is determined by the fast-decaying $\Delta\varepsilon''_{\text{ib}}$. The green curve in Figure 3a shows the results of numerical calculations according to the Supporting Information, section V. Good agreement between experimental and calculated dependences verifies that the modeled change in gold permittivity is correct. It can also be noted that the numerical spectrum is slightly sharper than the experimental one. As we neglect imperfections like minor angular divergence of the probe beam in modeling, the

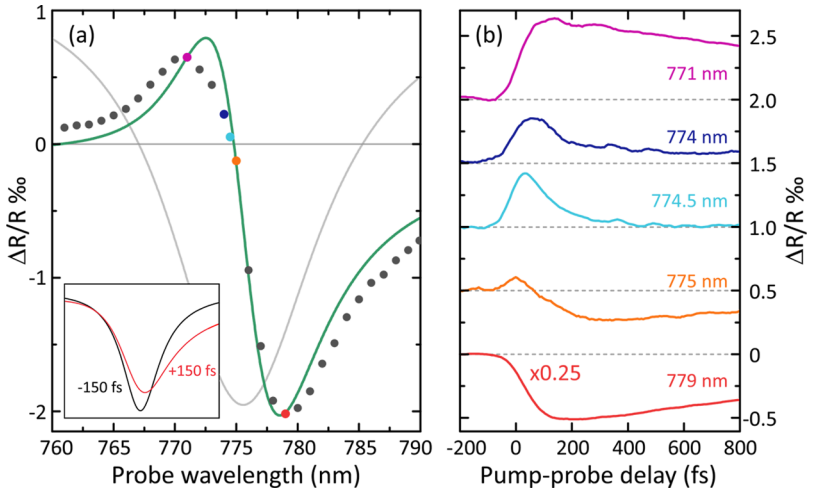

Figure 3. (a) Spectrum of the relative change in reflectance of the sample (dots) at τ_D = 200 fs. Green curve shows the result of numerical calculations. Gray line shows a TP resonance in reflectance. Inset shows a sketch of the TP resonance shift. (b) Transient reflectance of the sample measured at different wavelengths of the probe beam. Curves are vertically shifted by 0.5 ‰ for clarity.

DOI: 10.1021/acsphotonics.8b01792
ACS Photonics 2019, 6, 844−850

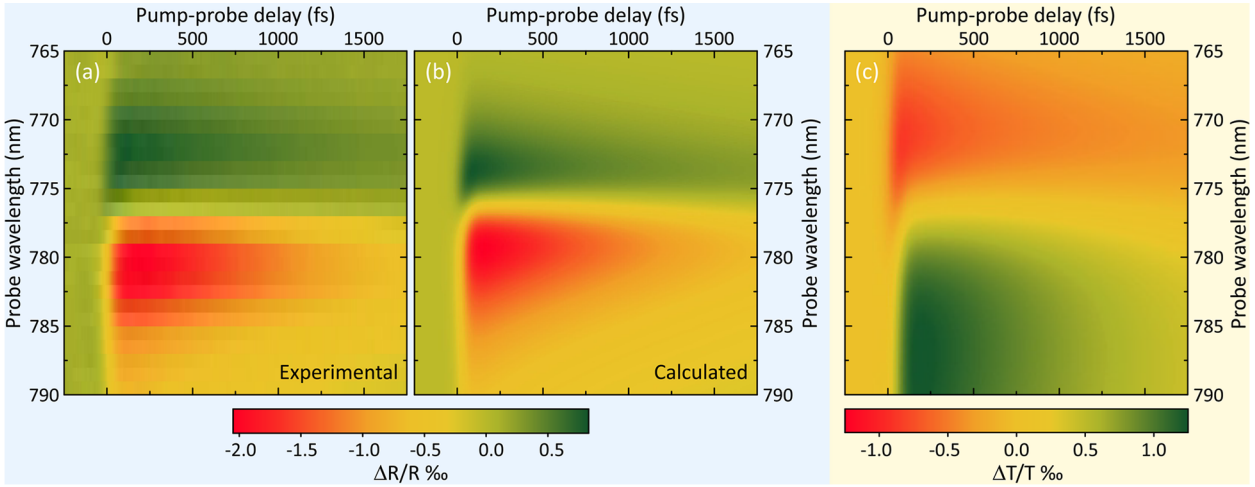

Figure 4. Experimentally measured (a) and numerically calculated (b) relative changes in the sample reflectance vs probe wavelength and the time delay between pump and probe pulses. (c) Calculated relative change in the sample transmittance vs probe wavelength and the time delay between pump and probe pulses.

calculated resonances are narrower. This highly likely explains the observed discrepancy.

Figure 3b shows transient reflectance at selected probe wavelengths around the TP resonance. Probing away from the resonance (pink and red curves) gives up to 20-fold larger values of $\Delta R/R$ as compared with gold. However, the decay times are at the picosecond scale, as they are governed by the electron−phonon coupling. At the probe wavelength of 779 nm (red curve), $\alpha'' = 0$, thus, $\Delta R/R(\tau)$ mimics $\Delta\varepsilon'(\tau)$. When the probe wavelength blueshifts, α'' begins to grow, while α' decreases. At the wavelength of 774 nm (blue curve), $\alpha' = 0$, so the transient reflectance has the shape of $\Delta\varepsilon''(\tau)$. At the wavelengths between, $\Delta R/R$ has a complex shape determined by the relative contributions from real and imaginary parts of the transient permittivity. For instance, at the probe wavelength of 775 nm (orange curve), reflectance shows a fast positive modulation, which is succeeded by the negative one, and the slow picosecond equilibration.

In bare metal films the similar picture is observed when probing near intrinsic resonances, for example, at the wavelengths around d−sp transition threshold.[42] However, in such a case, the dynamics of reflectance and transmittance is slower since one involves transitions to the long-living states close to Fermi energy. Another shortcoming is that wavelengths of the interband transitions in metals are close to the ultraviolet part of the spectrum. The latter is inappropriate for the telecom and plasmonic applications. In contrast, engineering artificial resonances allows for shifting the wavelength of the pulse-limited modulation to the infrared spectral range.

The generalized results of the time-resolved reflectance spectroscopy of the PC−metal sample are presented in Figure 4a. The plot shows $\Delta R/R$ versus the probe wavelength and the time delay between pump and probe pulses. It can be seen that the wavelength dependence of $\Delta R/R$ has an asymmetric profile with the positive modulation at the short-wave side of the TP resonance and the negative modulation at the long-wave side. Temporal dynamics of the reflectance is also wavelength-dependent. This is attributed to the different ratios of α'/α'' at different wavelengths, as was discussed earlier. It should also be noted that $\Delta R/R$ rapidly approaches zero when the probe wavelength is blueshifted from the TP resonance. In contrast, at the long-wave side of the resonance, the reflectance modulation is nonzero in a wider spectral range. This is a direct consequence of the α'' spectral dependence. Numerical simulations of the sample $\Delta R/R$ versus probe wavelength and pump−probe delay are shown in Figure 4b. Calculated spectrum is in an excellent agreement with the experimental data.

Figure 4c shows a numerically calculated time-resolved spectrum of the PC−metal sample $\Delta T/T$. Both reflectance and transmittance spectra have derivative-like shapes in the vicinity of TP resonance. While ΔR is being positive at the short-wave edge of the resonance and negative at the long-wave side, ΔT exhibits an opposite behavior. This is expected since TP resonance manifests as a dip in the $R(\lambda)$ and as a peak in the $T(\lambda)$. Moreover, the spectrum of the $\Delta T/T$ is more symmetric and displays comparable values of modulation at both sides of the resonance. The spectrum of $\Delta T/T$ follows the spectral dependences of β' and β'', as demonstrated in the Supporting Information, section IV.

As it is seen from Figure 4, background-free ultrafast modulation can be achieved in both reflection and transmission geometries. An important fact is that magnitudes and specific switching times are the same for $\Delta R/R$ and $\Delta T/T$. However, the sign of the modulation is opposite (positive for R, negative for T) and wavelengths of the ultrafast modulation differ by 1.5 nm. This feature looks promising for the all-optical demultiplexing.

As the last step, we measured the temporal dynamics of the sample broadband reflectance and transmittance, collecting an integral probe signal at all wavelengths. Black dots in Figure 5a show a normalized $\Delta R/R$ of the sample, while orange dots show the same of the bare gold film. First, it should be noted that the magnitude of the sample $\Delta R/R$ is 15× larger than the one of the gold film. Second, the transient reflectance of the sample has the same behavior as the gold one. The initial rise of the reflectance occurs within 250 fs and is followed by the exponential decay. The decay constant found from the single-exponential fit is 1.2 ps which is in a good agreement with the previously reported values for gold.[21]

Temporal dependence of the relative change in the sample transmittance $\Delta T/T$ shown in Figure 5b has a more peculiar behavior. After the initial excitation, ΔT exhibits an ultrafast pulse-limited spike. The spike occurs at the same time scale of

DOI: 10.1021/acsphotonics.8b01792
ACS Photonics 2019, 6, 844−850

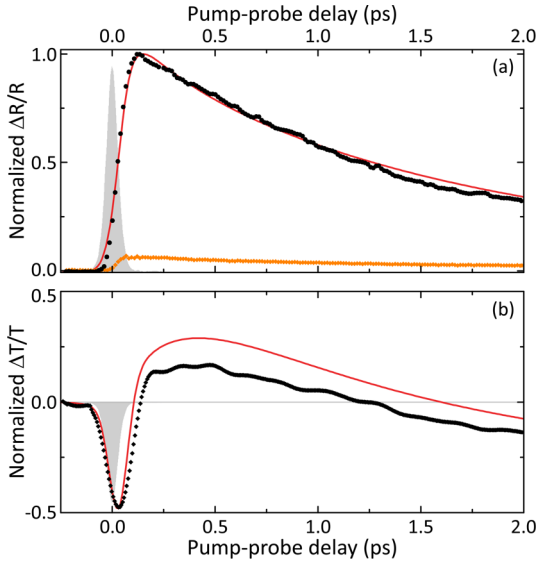

Figure 5. Transient reflectance (a) and transmittance (b) of the sample. Orange dots show a transient reflectance of the bare gold film. Shaded areas show the pump−probe cross-correlation. Solid red curves show the results of numerical calculations.

250 fs as the initial rise of ΔR and is followed by a slow picosecond relaxation. The maximum of the initial fast transmittance modulation occurs 30 fs after the peak of the pump−probe cross-correlation. This delay is most likely related to the finite lifetime of the TP, which equals to 32 fs for a TE-polarized light incident at the angle of 25°.[43]

As it was mentioned, the coefficients α and β for a bare gold film are almost independent of the probe wavelength in the infrared region. The transient reflectance of the gold is determined by both the $\Delta\varepsilon'$ and $\Delta\varepsilon''$, while the transient transmittance takes the shape of the $\Delta\varepsilon'(\tau)$. However, ultrafast features of $\Delta\varepsilon''_{\text{ib}}$ are cloaked by much more notable $\Delta\varepsilon'$, since α and β have about the same magnitude. In contrast, for the PC−metal sample spectra of α and β are nonmonotonic and sign-changing. Thus, the transient broadband $\Delta R/R$ and $\Delta T/T$ become the complex combination of $\Delta\varepsilon'$ and $\Delta\varepsilon''$.

At wavelengths in the vicinity of TP resonance, α' is 10× larger than α'', which means that the $\Delta R/R$ is dominated by changes in ε'. At the same time, $\Delta T/T(\tau)$ demonstrates transient features of both ε' and ε'' as β'' is twice as large as β' and has the opposite sign. The ultrafast spike in transient transmittance visible in Figure 5b at the time scale of ±150 fs occurs because $\Delta T/T(\tau)$ essentially reflects $\Delta\varepsilon''(\tau)$ as the latter grows much faster than the $\Delta\varepsilon'(\tau)$. After 150 fs $\Delta\varepsilon'$ reaches its maximum, becomes 8× larger than the $\Delta\varepsilon''$, and starts to decay exponentially. When $\Delta\varepsilon'$ falls below approximately $2\Delta\varepsilon''$, $\Delta T/T$ of the PC−metal sample becomes negative and approaches constant value determined by the modulation of ε'' due to the heating of the gold lattice. The complete relaxation to the unperturbed value takes several dozens of picoseconds and is not shown here.

Using calculated values of $\hat{\varepsilon}_{\text{Me}}$ we have modeled the transient optical response of the PC−metal sample using a procedure, described in the Supporting Information, section V. The results of numerical calculations shown in Figure 5 with solid curves are in an excellent agreement with the experimental data.

The presence of the picosecond background in the broadband $\Delta T/T$ (Figure 5b) is determined by the ratio of $\sum_\lambda \beta'$ and $\sum_\lambda \beta''$ over all probe wavelengths λ. Coefficients, in turn, are defined by the geometry and material properties of the sample. By adjusting thicknesses, materials, and number of layers, one can achieve background-free ultrafast modulation of the broadband transmittance of the PC−metal sample. On the other hand, for virtually any PC−metal sample, one can find wavelengths in the vicinity of the TP resonance at which $\alpha''/\alpha' = -\Delta\varepsilon'/\Delta\varepsilon''_{\text{intra}}$ or $\beta''/\beta' = -\Delta\varepsilon'/\Delta\varepsilon''_{\text{intra}}$. At those wavelengths, $\Delta R/R$ and $\Delta T/T$, respectively, will exhibit a pulse-limited switching.

TP-supporting samples are compatible with the current CMOS technology and can be easily embedded into the on-chip photonic circuits. The biggest advantage of such samples is the ability to smoothly tune the wavelength of the TP resonance in the broad range around the design value. Thus, the operational wavelength range of the TP-switch is significantly larger than the one of the current nanoplasmonic switches. However, most of them can be complemented with a PC to support excitation of Tamm plasmon. In the discussed experiment, the permittivity of only the gold layer was modulated. Nevertheless, the magnitude of the broadband sample $\Delta R/R$ is significantly enhanced as compared with a bare gold. Broadband sample $\Delta T/T$ displayed the completely different dynamics with an ultrafast pulse-limited spike. Thus, PC−metal samples are promising candidates for expanding the scope of plasmonic and photonic devices. A background-free modulation can be significantly boosted if a nonlinear material is used for the topmost layer of a PC. Additional enhancement of the modulation can be achieved by the spatial localization of the pump field, for example, in the waveguide-like geometry.[29,44] Proper selection of the geometry and nonlinear materials[45] and using resonant pump scheme can guarantee full switching ($\Delta R \sim 0.5$) at pJ pump pulse energies.

In conclusion, we have demonstrated that PC−metal nanostructures can be used to achieve ultrafast reflectance and transmittance modulation at wavelengths around the Tamm-plasmon resonance. The resonant wavelength is defined by the sample geometry and can be efficiently tuned to the desired spectral range. Using pump−probe technique, we have shown that the magnitude of the sample broadband $\Delta R/R$ is 15× larger than the one of a bare gold film at the same fluence of the infrared pump. Moreover, we have shown that by choosing proper wavelength around TP resonance, dynamics and magnitude of the sample reflectance and transmittance can be arbitrarily tailored. Namely, at the wavelength of 774.5 nm, close to the resonance minimum, we observed background-free 150 fs switching with the magnitude of 4×10^{-4}. In contrast, at the wavelength of 779 nm, corresponding to the slope of the resonance, we observed modulation of 2‰ with a picosecond relaxation. We believe that the reported results are useful to improve the performance of integrated plasmonic devices, such as switches, modulators, and demultiplexers.

METHODS

Samples. The sample under study was a one-dimensional photonic crystal comprising SiO_2 and ZrO_2 layers and terminated with a semitransparent 30 nm thick gold film. Layer thicknesses were 110 and 145 nm for ZrO_2 and SiO_2 layers, respectively. The thickness of the topmost SiO_2 layer was 220 nm to adjust the TP excitation wavelength to the range of the used laser. The sample was made by successive e-

DOI: 10.1021/acsphotonics.8b01792
ACS Photonics 2019, 6, 844−850

beam deposition of layers to the fused silica substrate. Using scanning electron microscopy, we have confirmed that the layer thicknesses are uniform across the sample and that the deviation from the target thicknesses is less than 1 nm. A bare 30 nm thick gold film on the same substrate was also prepared to be used for the reference measurements.

■ ASSOCIATED CONTENT

Supporting Information

The Supporting Information is available free of charge on the ACS Publications website at DOI: 10.1021/acsphotonics.8b01792.

Detailed description of the experimental procedures and numerical calculations (PDF)

■ AUTHOR INFORMATION

Corresponding Author

*E-mail: afinogenov@nanolab.phys.msu.ru.

ORCID

Boris I. Afinogenov: 0000-0002-5382-3647

Andrey A. Fedyanin: 0000-0003-4708-6895

Notes

The authors declare no competing financial interest.

■ ACKNOWLEDGMENTS

The authors thank E. P. Gilshteyn for helping with scanning electron microscopy characterization and B. Lukyanchuk for the stimulating discussions. The research was financially supported by the Ministry of Education and Science of the Russian Federation (Grant No. 14.W03.31.0008, experimental measurements), the Russian Foundation for Basic Research (Grant Nos. 17-02-01419 and 17-08-01716, setup development), the Russian Science Foundation (Grant No. 15-12-00065, numerical calculations), and MSU Quantum Technology Center.

■ REFERENCES

(1) Wurtz, G. A.; Pollard, R.; Hendren, W.; Wiederrecht, G. P.; Gosztola, D. J.; Podolskiy, V. A.; Zayats, A. V. Designed ultrafast optical nonlinearity in a plasmonic nanorod metamaterial enhanced by nonlocality. *Nat. Nanotechnol.* **2011**, *6*, 107.

(2) Baida, H.; Mongin, D.; Christofilos, D.; Bachelier, G.; Crut, A.; Maioli, P.; Del Fatti, N.; Vallée, F. Ultrafast nonlinear optical response of a single gold nanorod near its surface plasmon resonance. *Phys. Rev. Lett.* **2011**, *107*, 057402.

(3) Wang, X.; Morea, R.; Gonzalo, J.; Palpant, B. Coupling localized plasmonic and photonic modes tailors and boosts ultrafast light modulation by gold nanoparticles. *Nano Lett.* **2015**, *15*, 2633−2639.

(4) Harutyunyan, H.; Martinson, A. B. F.; Rosenmann, D.; Khorashad, L. K.; Besteiro, L. V.; Govorov, A. O.; Wiederrecht, G. P. Anomalous ultrafast dynamics of hot plasmonic electrons in nanostructures with hot spots. *Nat. Nanotechnol.* **2015**, *10*, 770.

(5) Pohl, M.; Belotelov, V. I.; Akimov, I. A.; Kasture, S.; Vengurlekar, A. S.; Gopal, A. V.; Zvezdin, A. K.; Yakovlev, D. R.; Bayer, M. Plasmonic crystals for ultrafast nanophotonics: optical switching of surface plasmon polaritons. *Phys. Rev. B: Condens. Matter Mater. Phys.* **2012**, *85*, 081401.

(6) MacDonald, K. F.; Sámson, Z. L.; Stockman, M. I.; Zheludev, N. I. Ultrafast active plasmonics. *Nat. Photonics* **2009**, *3*, 55.

(7) Fang, X.; Tseng, M. L.; Ou, J.-Y.; MacDonald, K. F.; Tsai, D. P.; Zheludev, N. I. Ultrafast all-optical switching via coherent modulation of metamaterial absorption. *Appl. Phys. Lett.* **2014**, *104*, 141102.

(8) Gholipour, B.; Zhang, J.; MacDonald, K. F.; Hewak, D. W.; Zheludev, N. I. An all-optical, non-volatile, bidirectional, phase-change meta-switch. *Adv. Mater.* **2013**, *25*, 3050−3054.

(9) Shorokhov, A. S.; Okhlopkov, K. I.; Reinhold, J.; Helgert, C.; Shcherbakov, M. R.; Pertsch, T.; Fedyanin, A. A. Ultrafast control of third-order optical nonlinearities in fishnet metamaterials. *Sci. Rep.* **2016**, *6*, 28440.

(10) Nozaki, K.; Tanabe, T.; Shinya, A.; Matsuo, S.; Sato, T.; Taniyama, H.; Notomi, M. Sub-femtojoule all-optical switching using a photonic-crystal nanocavity. *Nat. Photonics* **2010**, *4*, 477.

(11) Moille, G.; Combrié, S.; Morgenroth, L.; Lehoucq, G.; Neuilly, F.; Hu, B.; Decoster, D.; de Rossi, A. Integrated all-optical switch with 10 ps time resolution enabled by ALD. *Laser Photon. Rev.* **2016**, *10*, 409−419.

(12) Musorin, A. I.; Sharipova, M. I.; Dolgova, T. V.; Inoue, M.; Fedyanin, A. A. Ultrafast Faraday rotation of slow light. *Phys. Rev. Appl.* **2016**, *6*, 024012.

(13) Piccione, B.; Cho, C.-H.; Van Vugt, L. K.; Agarwal, R. All-optical active switching in individual semiconductor nanowires. *Nat. Nanotechnol.* **2012**, *7*, 640.

(14) Born, B.; Krupa, J. D. A.; Geoffroy-Gagnon, S.; Holzman, J. F. Integration of photonic nanojets and semiconductor nanoparticles for enhanced all-optical switching. *Nat. Commun.* **2015**, *6*, 8097.

(15) Shcherbakov, M. R.; Vabishchevich, P. P.; Shorokhov, A. S.; Chong, K. E.; Choi, D.-Y.; Staude, I.; Miroshnichenko, A. E.; Neshev, D. N.; Fedyanin, A. A.; Kivshar, Y. S. Ultrafast all-optical switching with magnetic resonances in nonlinear dielectric nanostructures. *Nano Lett.* **2015**, *15*, 6985−6990.

(16) Wang, Q.; Rogers, E. T. F.; Gholipour, B.; Wang, C.-M.; Yuan, G.; Teng, J.; Zheludev, N. I. Optically reconfigurable metasurfaces and photonic devices based on phase change materials. *Nat. Photonics* **2016**, *10*, 60.

(17) Chu, C. H.; Tseng, M. L.; Chen, J.; Wu, P. C.; Chen, Y.-H.; Wang, H.-C.; Chen, T.-Y.; Hsieh, W. T.; Wu, H. J.; Sun, G.; Tsai, D. P. Active dielectric metasurface based on phase-change medium. *Laser Photon. Rev.* **2016**, *10*, 986−994.

(18) Shcherbakov, M. R.; Liu, S.; Zubyuk, V. V.; Vaskin, A.; Vabishchevich, P. P.; Keeler, G.; Pertsch, T.; Dolgova, T. V.; Staude, I.; Brener, I.; Fedyanin, A. A. Ultrafast all-optical tuning of direct-gap semiconductor metasurfaces. *Nat. Commun.* **2017**, *8*, 17.

(19) Hohlfeld, J.; Wellershoff, S.-S.; Güdde, J.; Conrad, U.; Jähnke, V.; Matthias, E. Electron and lattice dynamics following optical excitation of metals. *Chem. Phys.* **2000**, *251*, 237−258.

(20) Del Fatti, N.; Voisin, C.; Achermann, M.; Tzortzakis, S.; Christofilos, D.; Vallée, F. Nonequilibrium electron dynamics in noble metals. *Phys. Rev. B: Condens. Matter Mater. Phys.* **2000**, *61*, 16956.

(21) Sun, C.-K.; Vallee, F.; Acioli, L.; Ippen, E. P.; Fujimoto, J. G. Femtosecond investigation of electron thermalization in gold. *Phys. Rev. B: Condens. Matter Mater. Phys.* **1993**, *48*, 12365.

(22) Sasin, M. E.; Seisyan, R. P.; Kalitteevski, M. A.; Brand, S.; Abram, R. A.; Chamberlain, J. M.; Egorov, A. Y.; Vasil'ev, A. P.; Mikhrin, V. S.; Kavokin, A. V. Tamm plasmon polaritons: Slow and spatially compact light. *Appl. Phys. Lett.* **2008**, *92*, 251112.

(23) Badugu, R.; Lakowicz, J. R. Tamm state-coupled emission: effect of probe location and emission wavelength. *J. Phys. Chem. C* **2014**, *118*, 21558−21571.

(24) Auguié, B.; Bruchhausen, A.; Fainstein, A. Critical coupling to Tamm plasmons. *J. Opt.* **2015**, *17*, 035003.

(25) Symonds, C.; Azzini, S.; Lheureux, G.; Piednoir, A.; Benoit, J. M.; Lemaitre, A.; Senellart, P.; Bellessa, J. High quality factor confined Tamm modes. *Sci. Rep.* **2017**, *7*, 3859.

(26) Azzini, S.; Lheureux, G.; Symonds, C.; Benoit, J.-M.; Senellart, P.; Lemaitre, A.; Greffet, J.-J.; Blanchard, C.; Sauvan, C.; Bellessa, J. Generation and spatial control of hybrid Tamm plasmon/surface plasmon modes. *ACS Photonics* **2016**, *3*, 1776−1781.

(27) Pankin, P. S.; Vetrov, S. Y.; Timofeev, I. V. Tunable hybrid Tamm-microcavity states. *J. Opt. Soc. Am. B* **2017**, *34*, 2633−2639.

(28) Lheureux, G.; Azzini, S.; Symonds, C.; Senellart, P.; Lemaître, A.; Sauvan, C.; Hugonin, J.-P.; Greffet, J.-J.; Bellessa, J. Polarization-

DOI: 10.1021/acsphotonics.8b01792
ACS Photonics 2019, 6, 844−850

controlled confined Tamm plasmon lasers. *ACS Photonics* **2015**, *2*, 842−848.
(29) Symonds, C.; Lheureux, G.; Hugonin, J.-P.; Greffet, J.-J.; Laverdant, J.; Brucoli, G.; Lemaitre, A.; Senellart, P.; Bellessa, J. Confined Tamm plasmon lasers. *Nano Lett.* **2013**, *13*, 3179−3184.
(30) Brückner, R.; Zakhidov, A. A.; Scholz, R.; Sudzius, M.; Hintschich, S. I.; Fröb, H.; Lyssenko, V. G.; Leo, K. Phase-locked coherent modes in a patterned metal−organic microcavity. *Nat. Photonics* **2012**, *6*, 322.
(31) Afinogenov, B. I.; Popkova, A. A.; Bessonov, V. O.; Lukyanchuk, B.; Fedyanin, A. A. Phase matching with Tamm plasmons for enhanced second-and third-harmonic generation. *Phys. Rev. B: Condens. Matter Mater. Phys.* **2018**, *97*, 115438.
(32) Zhang, W. L.; Yu, S. F. Bistable switching using an optical Tamm cavity with a Kerr medium. *Opt. Commun.* **2010**, *283*, 2622−2626.
(33) Afinogenov, B. I.; Bessonov, V. O.; Fedyanin, A. A. Second-harmonic generation enhancement in the presence of Tamm plasmon-polaritons. *Opt. Lett.* **2014**, *39*, 6895−6898.
(34) Kumar, S.; Shukla, M. K.; Maji, P. S.; Das, R. Self-referenced refractive index sensing with hybrid-Tamm-plasmon-polariton modes in sub-wavelength analyte layers. *J. Phys. D: Appl. Phys.* **2017**, *50*, 375106.
(35) Huang, S.-G.; Chen, K.-P.; Jeng, S.-C. Phase sensitive sensor on Tamm plasmon devices. *Opt. Mater. Express* **2017**, *7*, 1267−1273.
(36) Kumar, S.; Maji, P. S.; Das, R. Tamm-plasmon resonance based temperature sensor in a Ta_2O_5/SiO_2 based distributed Bragg reflector. *Sens. Actuators, A* **2017**, *260*, 10−15.
(37) Yang, Z.-Y.; Ishii, S.; Yokoyama, T.; Dao, T. D.; Sun, M.-G.; Nagao, T.; Chen, K.-P. Tamm plasmon selective thermal emitters. *Opt. Lett.* **2016**, *41*, 4453−4456.
(38) Yang, Z.-Y.; Ishii, S.; Yokoyama, T.; Dao, T. D.; Sun, M.-G.; Pankin, P. S.; Timofeev, I. V.; Nagao, T.; Chen, K.-P. Narrowband wavelength selective thermal emitters by confined Tamm plasmon polaritons. *ACS Photonics* **2017**, *4*, 2212−2219.
(39) Badugu, R.; Descrovi, E.; Lakowicz, J. R. Radiative decay engineering 7: Tamm state-coupled emission using a hybrid plasmonic-photonic structure. *Anal. Biochem.* **2014**, *445*, 1−13.
(40) Zhang, D.; Qiu, D.; Chen, Y.; Wang, R.; Zhu, L.; Wang, P.; Ming, H.; Badugu, R.; Stella, U.; Descrovi, E.; Lakowicz, J. R. Coupling of Fluorophores in Single Nanoapertures to Tamm Plasmon Structures. *J. Phys. Chem. C* **2019**, *123*, 1413−1420.
(41) Groeneveld, R. H. M.; Sprik, R.; Lagendijk, A. Femtosecond spectroscopy of electron-electron and electron-phonon energy relaxation in Ag and Au. *Phys. Rev. B: Condens. Matter Mater. Phys.* **1995**, *51*, 11433.
(42) Sun, C.-K.; Vallée, F.; Acioli, L. H.; Ippen, E. P.; Fujimoto, J. G. Femtosecond-tunable measurement of electron thermalization in gold. *Phys. Rev. B: Condens. Matter Mater. Phys.* **1994**, *50*, 15337.
(43) Afinogenov, B. I.; Popkova, A. A.; Bessonov, V. O.; Fedyanin, A. A. Measurements of the femtosecond relaxation dynamics of Tamm plasmon-polaritons. *Appl. Phys. Lett.* **2016**, *109*, 171107.
(44) Melentiev, P. N.; Afanasiev, A. E.; Kuzin, A. A.; Zablotskiy, A. V.; Balykin, V. I. Giant enhancement of two photon induced luminescence in metal nanostructure. *Opt. Express* **2015**, *23*, 11444−11452.
(45) Molyneux, S.; Kar, A. K.; Wherrett, B. S.; Axon, T. L.; Bloor, D. Near-resonant refractive nonlinearity in polydiacetylene 9-BCMU thin films. *Opt. Lett.* **1993**, *18*, 2093−2095.

DOI: 10.1021/acsphotonics.8b01792
ACS Photonics 2019, 6, 844−850